International Society for Rock Mechanics and Rock Engineering
Norwegian Group for Rock Mechanics

ISRM International Symposium
Eurock 2025 – Expanding the Underground Space
Trondheim, Norway, 16-20 June
ISBN 978-82-8208-079-8

Mechanical stability of salt caverns under intensive gas storage conditions using LOCAS and DISROC

H. Habbani & H. Djizanne
Ineris, Verneuil-en-Halatte, France
hajar.habbani@ineris.fr

B. Brouard
Brouard Consulting, Paris, France

A. Pouya
Navier Laboratory, Ecole des Ponts, Gustave Eiffel University, CNRS, Marne la Vallée, France

Abstract

In gas storage operations, injection and withdrawal rates can reach high levels to meet increasing demand. Salt caverns intensive exploitation methods introduce significant mechanical challenges, particularly wall spalling. Spalling involves the detachment of plates or blocks from the cavern walls or roof, occurring with minimal volume loss, unlike progressive closure through creep. This study focuses on the detachment of overhanging blocks within specific salt caverns. Wall spalling is of particular concern because it can compromise the structural stability of the caverns, damaging well tubing posing risks to both the safety and the efficiency of storage operations. This article explores the mechanical stability of salt caverns using two finite element software. LOCAS software identifies potential failure zones in continuous media. It helps to examine damage initiation due to salt dilation and the onset of effective tensile stresses at the cavern wall. Dilatancy refers to the volume increase accompanying material deformation under stress, leading to microcracks formation. DISROC software simulates crack initiation and propagation for detailed failure analysis. It employs joint element model to visualize failure mechanisms in the selected cavern blocks. Simulating crack formation and propagation at the joints between blocks, offers a detailed perspective on how failure develop and extend within the cavern structure. These two methods are compared to assess the onset of damage and associated mechanisms in salt caverns under intensive gas storage conditions.

Keywords

Fracture mechanics, salt cavern, numerical computations, DISROC, LOCAS

1 Introduction

Underground gas storage (UGS) in salt caverns plays a pivotal role in meeting growing energy demands, whether for natural gas, hydrogen, or compressed air. Salt caverns, typically located at depths of 300 to 2,500 meters, are valued for their low permeability and structural stability, making them ideal for gas storage. However, the fluctuating and intensive energy demands require frequent cycles of gas injection and withdrawal, subjecting the caverns to significant mechanical stress. Pressure variations during these cycles can alter the rock salt mechanical behaviour, leading to microcracks formation and stress redistribution within the cavern wall. Over time, these processes may compromise mechanical stability, increasing the risk of localized failures such as spalling or block detachment. Understanding these phenomena is crucial to ensuring the long-term stability and safety of these storage facilities. This paper focuses on the challenges associated with the aggressive exploitation of salt caverns, particularly wall spalling, detachment of blocks or plates from cavern walls or roofs. The study investigates two methods for assessing damage initiation and rupture mechanisms in these caverns. The first method applies salt dilation and the onset of effective tensile stresses damage analyses, grounded in continuum mechanics principles for rock salt. The second method complements this by using joint-enriched finite element analysis (JFEM), incorporating a cohesive zone model to simulate crack nucleation and propagation at joint interfaces. Together, these approaches aim to enhance understanding of failure mechanisms at salt cavern call, with particular emphasis on mechanical stress effects.

2 Review of observations from real caverns

Fast cycling in the context of UGS in salt cavern, has often revealed significant mechanical stability challenges including block detachment, spalling and consistent volume loss. This section of the paper highlights specific cases in the literature where such mechanical instabilities have been observed.

The Kiel 101 cavern in Germany, located at depths between 1,305 m and 1,400 m, is an example of instability due to a fast depressurization. The cavern, situated in a salt formation with high levels of insoluble material, developed a significant sump at its base. During a pressure test, the cavern roof failed when the pressure was decreased from 13.1 MPa to 6.5 MPa in five days (Röhr 1974; Bérest et al. 2012). Sonar surveys revealed a significant decrease in the cavern accessible volume as a result of the rapid pressure drop. The failure was attributed to the combined effects of rapid depressurization and the heterogeneous nature of the salt formation.

A similar phenomenon was observed at the Eminence Salt Dome in Mississippi, USA. The cavern, situated at depths ranging from 1,725 m to 2,000 m, experienced severe deformation following pressure cycling. Initially, gas was injected, and the gas pressure was reduced to 6 MPa. After being maintained at this level for some time, the pressure was increased to 28 MPa. A similar pressure cycle was performed later, during which large volume losses were suspected. After two years, sonar surveys revealed a 40% reduction in cavern volume, accompanied by a rise in the cavern bottom of 36 m (Coates et al. 1983); while block falls were suspected (Bérest et al. 2012). In addition to possible block falls, Bérest et al. (1986) noted that the asymmetric deformation likely resulted from higher overburden pressure and elevated temperatures in the lower rock mass, which contributed to the cavern mechanical instability.

At Tersanne, the TE02 cavern experienced significant volume loss after repeated pressure cycles. Approximately one-third of its volume was lost, and the cavern bottom rose by 5.8 m, primarily due to the detachment of overhanging blocks identified in earlier sonar surveys (Bérest et al. 2012). Salt creep deformation also contributed to the instability, as indicated by smoother sonar profiles observed in subsequent surveys.

In contrast, the Huntorf CAES (Compressed Air Energy Storage) caverns in Germany exhibited an initial phase of instability marked by the detachment of salt blocks, causing the cavern bottom to rise by 16 m (Crotogino et al. 2001; Djizanne 2014). This initial instability was attributed to the loss of buoyancy caused by replacing brine with gas. However, once adjusted to operational conditions, these caverns demonstrated long-term stability over several decades, with laser sonar surveys confirming minimal further changes attributable to block falls (Quast 1983; Crotogino et al. 2001). Additionally, when cavern NK1 was expanded to atmospheric pressure, a laser tool survey revealed practically no deviation compared to the original conditions after more than 20 years of operation (Crotogino et al. 2001).

3 Numerical modelling

The numerical modelling presented in this paper is performed using two software: LOCAS (Brouard et al. 2022), a finite element code that predicts gas or liquid-filled caverns behaviour with fully coupled thermo-hydromechanical computations, and DISROC (Fracsima, 2016), a finite element code enriched with joint elements, dedicated to modelling of coupled thermo-hydromechanical phenomena in materials and structures containing discontinuities. LOCAS identifies potential failure zones in continuous media, while DISROC simulates crack initiation and propagation for detailed failure analysis. An axisymmetric cavern with a volume of 329,489 m^3 is considered (see Fig. 1a). The cavern has a height of 150 *m*, an average width of 71 *m*, and its top is located at a depth of 650 *m*. The chosen shape is based on the Huntorf NK1 cavern design, characterized by its overhanging block structure (Quast 1983, Djizanne et al. 2014).

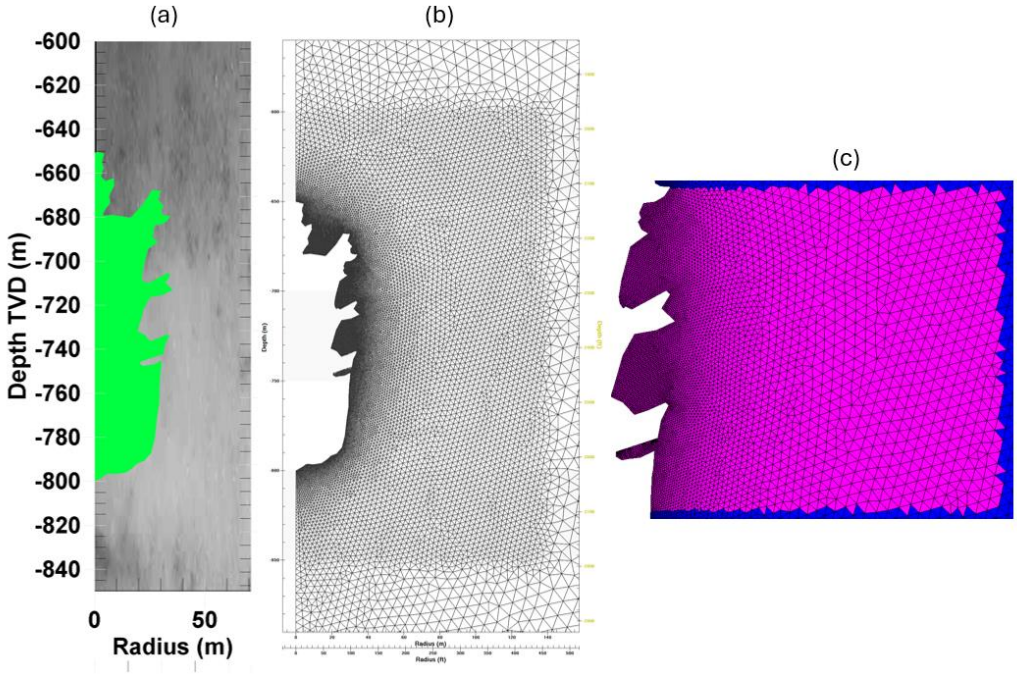

Fig. 1*(a)* Cavern shape inspired from the Huntorf NK1 sonar; *(b)* cavern meshing model, and *(c)* joints elements area.

The axisymmetric model incorporates the following boundary conditions: no radial displacement along the centerlines, geostatic pressure applied along the outer radius, and no vertical displacement along the bottom surface. The meshing is subdivided into three parts: close to the cavern wall (5 m-thick), with an increased high-density area where the maximum distance between nodes on the cavern wall is 0.5 m. Then, a high-density area follows, where the maximum size of elements is 3 m. And a low-density area where the maximum size of elements is 10 m (see Fig. 1b). The number of mesh elements is 52,828, including triangular and joint elements. Joint elements are generated close to the cavern wall in an area that includes the three overhanging blocks, according to the size of the model (1,000 m x 200 m). (see Fig. 1c) in order to simulate the nucleation and propagation of cracks contributing on spalling. The pre-processor DISCRAC enables splitting nodes of the initial mesh (see Fig. 1b) and creating a new mesh with joint elements to allow displacement discontinuities as presented in Tounsi et al. (2020).

4 Constitutive modelling

4.1 Continuum mechanics

The mechanical behaviour of rock salt exhibits significant nonlinearity and varies depending on the type and duration of applied stress. Under short-term compression tests, rock salt demonstrates elastic-ductile properties, while it behaves as an elastic-brittle material under tensile stress. Over extended periods, rock salt flows like a viscous fluid. This complex behaviour categorizes rock salt as elasto-viscoplastic, with pronounced nonlinearity and temperature sensitivity. Salt creep behaviour is captured in this paper by the Norton-Hoff (N-H) law or “power law”; it establishes a relationship between strain, deviatoric stress, and temperature during the steady-state phase, expressed as a power-law dependence of stress, where the strain rate increases with temperature following an Arrhenius law (Norton, 1929). The constitutive behaviour of the salt rock mass can be written as:

$$\dot{\varepsilon}_{ij} = \dot{\varepsilon}^{el} + \dot{\varepsilon}^{vp} \quad (1)$$

$$\dot{\varepsilon}^{el} = \frac{1+\nu}{E}\dot{\sigma}_{ij} - \frac{\nu}{E}\dot{\sigma}_{ij}\delta_{ij} \quad (2)$$

$$\dot{\varepsilon}^{vp} = \frac{3}{2} A\, e^{-(\frac{Q}{RT})} (\sqrt{3J_2})^{n-1} s_{ij} \quad (3)$$

Eq.3 presents the viscoplastic component. The exponent (n) of the power law is in the range of 3-5, with $s_{ij} = \sigma_{ij} - \frac{1}{3}\sigma_{kk}\delta_{ij}$ is the deviatoric stress tensor with J_2 is the second invariant of the deviatoric stress tensor. The salt parameters considered in this paper are derived from the Etrez salt as mentioned by Djizanne (2014). The Table 1 presents the modelled rocks properties.

Table 1. Modelled rocks properties.

Rock	Constitutive law	Thickness (m)	Density (kg/ m³)	E (MPa)	ν (-)	A (MPa^{-n}/yr)	Q/R (K)	n
Overburden	Elastic	500	2,520	8,600	0.23	-	-	-
Salt	Norton Hoff	500	2,200	30,000	0.25	0.64	4,100	3.1

4.2 Fracture mechanics

The progressive weakening of rock strength and stiffness can lead to fractures, a process described using damage mechanics. In the constitutive model by Pouya and Bemani (2015), material damage, viewed as a yielding process, is integrated into a cohesive fracture framework. This framework assumes an infinitesimal cohesive zone ahead of the crack tip, where a cohesive constitutive law relates the stress tensor ($\underline{\sigma}$) to the displacement discontinuities ($\underline{u}$), comprising normal and tangential. The cohesive damage model governs fracture behaviour under compression, enforcing a non-penetration condition where the normal displacement (u_n) cannot exceed the initial aperture (e). The stress-displacement law, see Eq. 4, links stress ($\underline{\sigma}$), stiffness (K), and damage (D) to displacement ($\underline{u}$).

$$\underline{\sigma} = (1 - D).K.\underline{u} \quad (4)$$

The evolution of the damage variable D is governed by the elastic displacement limit u_0 of the cohesive fracture. When the normal displacement u_n is below u_0, D remains zero. As u_n exceeds u_0, D grows exponentially (see Fig. 2a), see Eq. 5. For an intact rock, $D = 0$ and for a completely damaged fracture, $D = 1$.

$$D = 1 - e^{-\frac{(u_n - u_0)}{\beta . u_0}}, u_n \geq u_0 \quad (5)$$

The parameter β defines material ductility, with values ranging from 0 to infinity. High values of β correspond to ductile materials, whereas β =0 represents a brittle material The failure criterion, dependent on D, is given by Eq. 6 (see Fig. 2b). Where C represents the cohesion on an intact cohesive fracture, τ and σ_n are the tangential and normal stresses, φ is the friction angle and σ_R the limit tensile strength of the intact joints.

$$F(\tau, \sigma_n, D) = \tau^2 - {\sigma_n}^2 tan^2\varphi + 2g(D)\,\sigma_c\,\sigma_n - g^2(D)\,C^2 ; \sigma_c = \frac{C^2 + \sigma_R^2 . tan^2\varphi}{2.\sigma_R} \quad (6)$$

$$g(D) = (1 - D)(1 - \beta . ln(1 - D)) \quad (7)$$

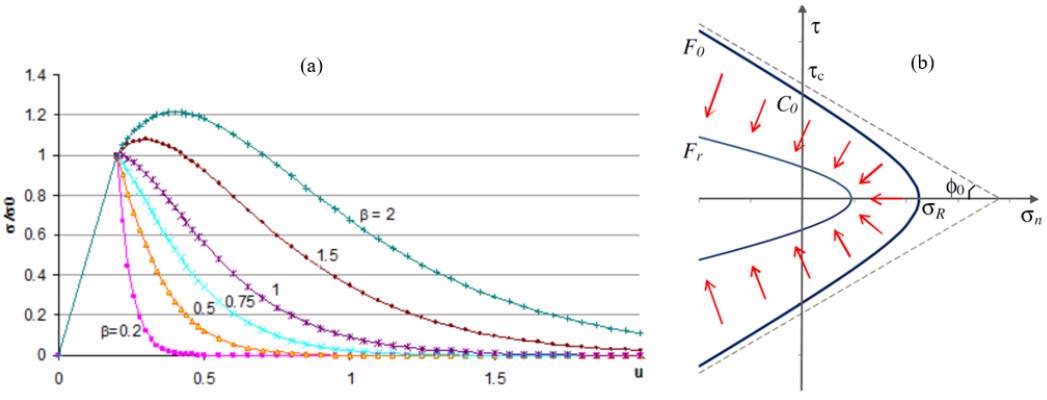

Fig. 2 *(a)* Stress-displacement in the cohesive zone model for different β values; *(b)* Evolution of the damage criterion to full joint failure (Ouraga et al. 2017).

The set of parameters for joints elements presented in the Table 2.

Table 2. Mechanical parameters of joints elements.

K_t (MPa.m^{-1})	K_n (MPa.m^{-1})	e (m)	σ_t (MPa)	C (MPa)	Φ (°)	k_t (MPa.m^{-1})	k_t (MPa.m^{-1})	β (-)
300,000	300,000	0.01	1.5	8	36.8	300	300	0.1

5 Modelling results

The main steps of the numerical computations presented in Fig. 3. First, at the end of the leaching, halmostatic pressure is applied to the cavern wall *(1)*. The second step corresponds to the completion of the debrining phase that lasts 100 days *(2)*. Subsequently, during the third step, the cavern reaches atmospheric pressure at the end of the withdrawal *(3)*. Finally, the fourth step presents the injection phase *(4)*.

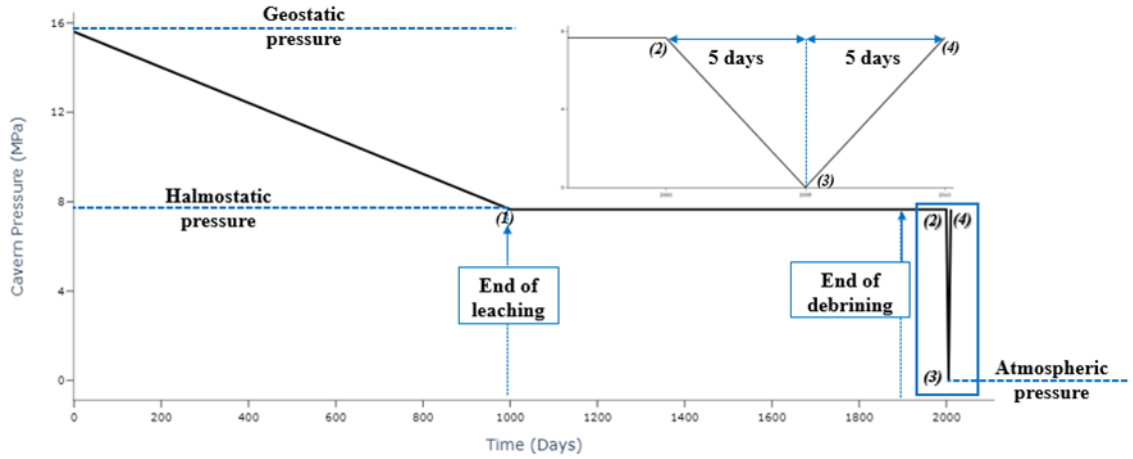

Fig. 3 Pressure evolution at the cavern top (-650 m).

5.1 Damage initiation due to salt dilation and the onset of tensile effective stresses

The continuum mechanics approach is used to assess the initiation of damage due to salt dilation and the onset of tensile effective stresses. The selected dilation criterion is the RD criterion with the Moss Bluff set of parameters (DeVries et al. 2003), represents salt failure as a function of mean stress, shear stress and Lode angle. Fig. 4 shows contour plots of the factor of safety (FoS) for three computation steps, rock salt is damaged when FoS is less than 1. A damaged area in the overhanging blocks is shown in magenta color at the end of the withdrawal due to rapid pressure drop in the cavern to atmospheric pressure (see Fig. 4. *(3)*). Salt dilation area is more prone to microcracks development. A dilation zone appears approximately 50 meters from the cavern wall (more than one radius). This dilation zone disappears at the end of the injection when the cavern is repressurized to halmostatic pressure (see Fig. 4. *(4)*).

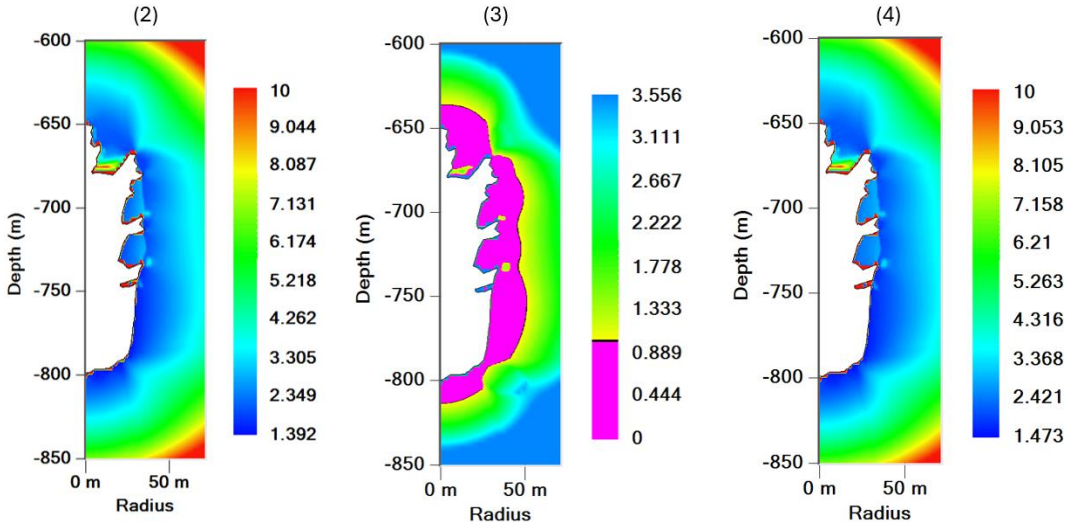

Fig. 4 Dilation contour plot at the end of debrining *(2)*; at the end of withdrawal *(3)* and at the end of injection *(4)* (LOCAS).

The onset of tensile effective stresses at the cavern wall indicates a potential for fractures or cracks formation (Djizanne et al. 2014, 2023). The tensile stress zone is particularly prominent at the end of the debrining, especially in larger zones within the overhanging blocks (Fig. 5). This may lead to a specific orientation of cracks within the blocks.

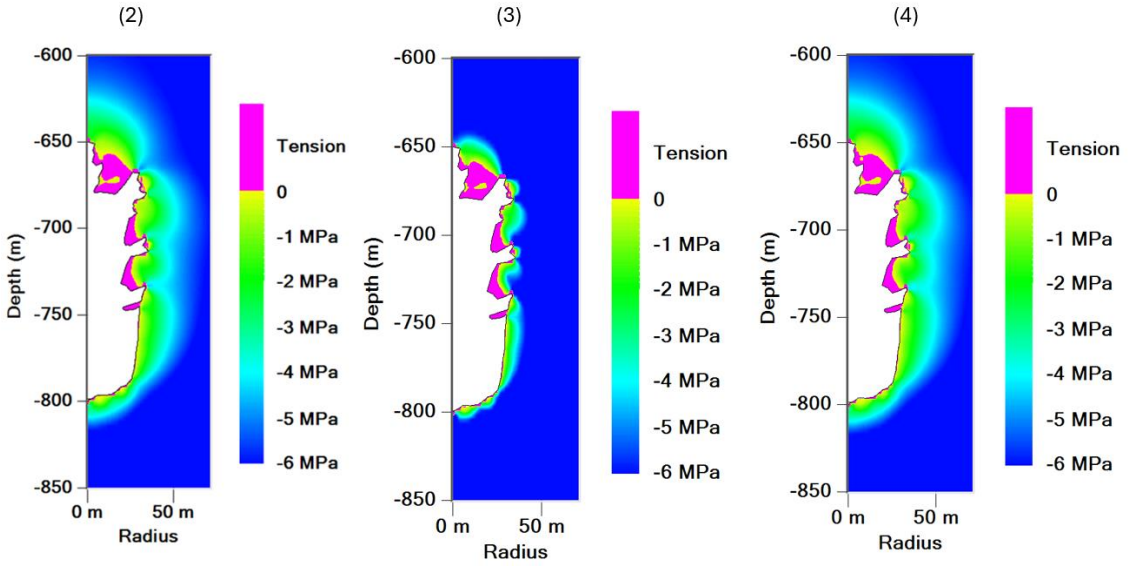

Fig. 5 Effective stress contour plot at the end of debrining *(2)*; at the end of withdrawal *(3)* and at the end of injection *(4)* (LOCAS).

5.2 A JFEM analysis for failure mechanism

A domain with generated joint elements extends up around 100 m from the cavern wall including overhanging blocks. A refined mesh was used to approximate energy dissipation for fracture nucleation accurately. A total of 18,026 joint elements were generated in an unstructured mesh format to avoid introducing any preferential direction and prevent overestimating energy. During the simulation of the withdrawal operation (step 3 on Fig. 3), a crack was initiated in the block located near the bottom of the cavern. This crack appeared after 2.4 days of depressurization, under a depressurization rate of -1.52 MPa/day. The crack initiation is marked by the fact that the normal stress on the joint, σ_n at the wall exceeds the salt tensile strength, which is considered 1.5 MPa (Fig. 6a) in this study, leading to brittle failure corresponding to an instantaneous dissipation of energy in the overhanging block due to a rapid drop. Between 2.4 and 2.5 days (equivalent to 2.4 hours), the crack propagates in a controlled and progressive manner. The figure illustrates the damage field of the joint during the stable crack propagation phase (Fig. 6c). Subsequently, excess energy triggers an unstable crack propagation, leading to the complete detachment of the block at 2.6 days of the withdrawal operation.

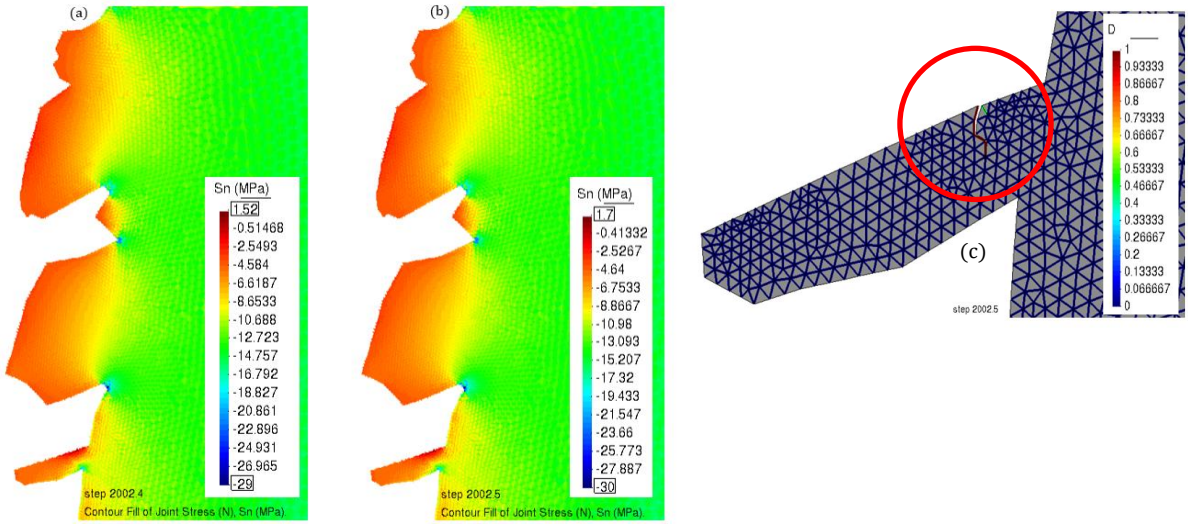

Fig. 6 Contour plots of normal joint stress at 2.4 days *(a)* and at 2.5 days of withdrawal operation *(b)*. *(c)* Joint damage field at 2.5 days of withdrawal operation (DISROC).

After simulating the detachment of the first block using the cohesive zone model, DISROC applies the excavation method to remove it. This process involves modifying the structure by altering the mesh geometry to reflect the removal or addition of parts. The excavation action transfers system states (e.g., stresses and displacements) from the previous mesh to the updated mesh by matching node coordinates, ensuring continuity in calculations despite changes in geometry.

After completing this step, the calculation of the withdrawal operation step will continue to assess the phenomenon of spalling in the remaining block. The results show the initiation of a crack in the upper block located approximately at a depth of -700 m, after 4.28 days of the withdrawal operation, when the normal stress on the joint σ_n, at the wall exceeded the tensile strength of the salt (1.5 MPa) (Fig. 7a). A portion of the block detached at 4.29 days, as presented in the damage field (Fig. 7b). At the end of the withdrawal operation, unstable crack propagation occurred, causing the cracks to penetrate the salt rock mass, with the upper part of the block tending to detach (Fig. 7c).

The numerical simulation showed the maximum extent of cracks in the rock mass to be approximately 48.16 m from the cavern wall (see Fig. 7). The observed crack propagation is approximately equivalent to the dilation zone estimated in the previous section using LOCAS.

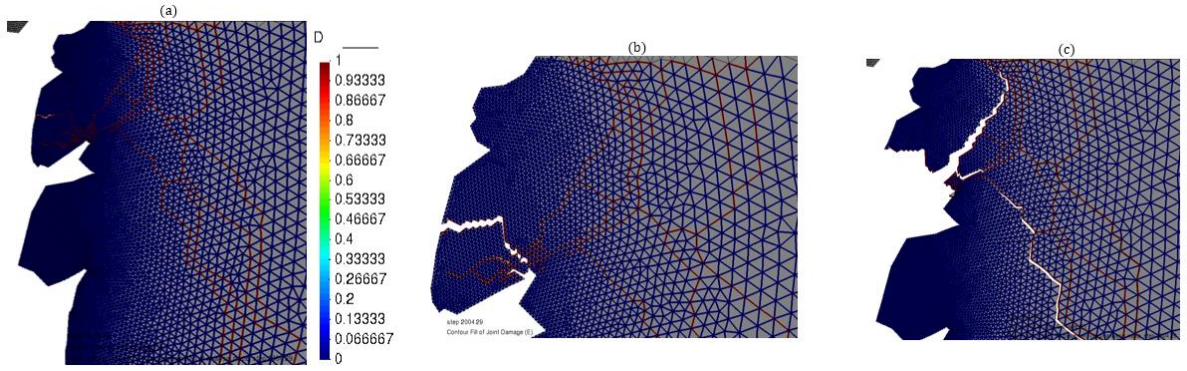

Fig. 7. Joint damage field with nucleation and propagation crack at 4.28 days (a); 4.29 days *(b)* and at the end of withdrawal operation *(c)* (x100 deformation) (DISROC).

Fig. 8 illustrates the outcomes of overhanging blocks detachment simulations. The progression of spalling is characterized by the sequential detachment of overhanging blocks, a first fall visualized at 2.6 days of withdrawal and the second fall at 4.29 days into the withdrawal.

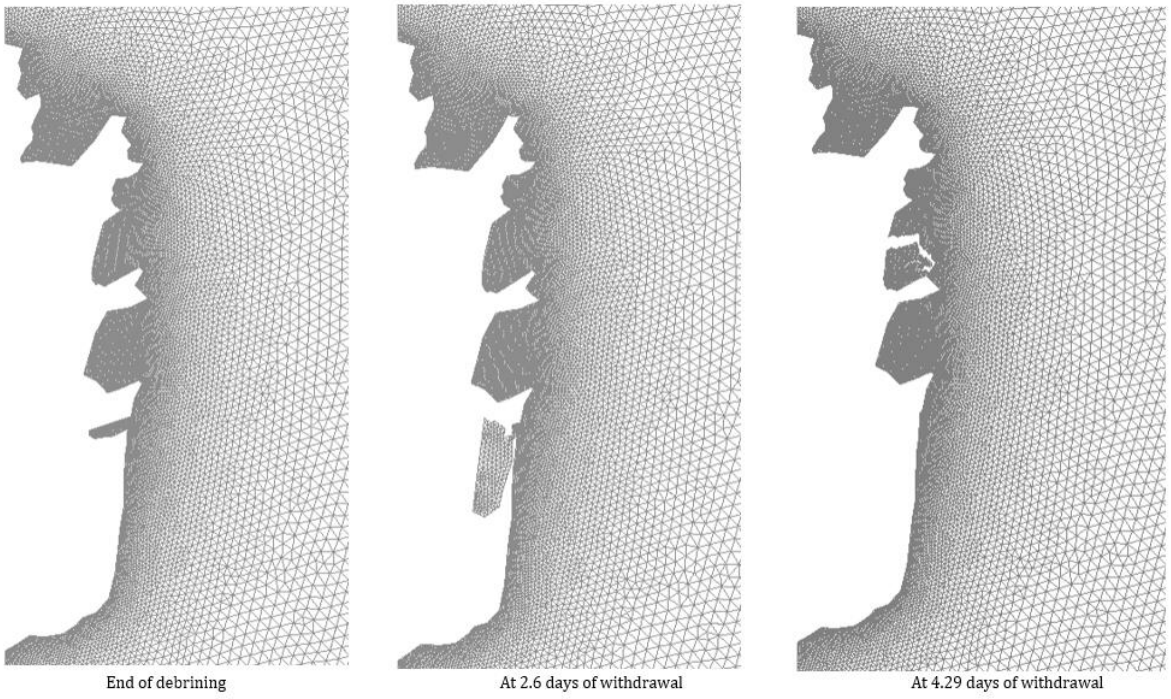

Fig. 8. Overhanging blocks falling outputs (DISROC).

6 Conclusion

This study provides a comprehensive analysis of the mechanical stability of salt caverns subjected to intensive gas storage conditions, with a particular focus on overhanging block failure and detachment. By employing two primary numerical approaches, the dilatancy and effective tensile stress analysis and the joint element model. The study offers valuable insights into the initiation and progression of damage mechanisms in rock salt at cavern scale. It also indicates that intensive gas storage operations, including rapid pressure cycles, could lead to the formation of dilation zone and tensile stress concentrations, particularly in overhanging blocks. Salt dilation revealed the occurrence of microcracks during the withdrawal phase, while the joint element model demonstrated the initiation and propagation of cracks, ultimately leading to block detachment. The numerical simulations confirmed that these failure mechanisms are highly influenced by rapid depressurization and stress redistribution within the surrounding rock mass.

Acknowledgments

This research was partly supported by funding from the Clean Hydrogen Partnership of the EU through the HyPSTER (n°101006751) and FrHyGe (n°101137892) projects.

References

Bandis S, Lumsden A, Barton N (1983) Fundamentals of rock joint deformation. Int J Rock Min Sci Geomech 4(6):249–268

Bérest P, Djizanne H, Brouard B, Hévin G (2012) Rapid depressurizations: Can they lead to irreversible damage? SMRI Spring Tech Conf, Regina, Canada, 63–86

Bérest P, Ghorechi M, Fauveau M, Lebitoux P (1986) Mechanisms of creep in gas storage caverns: effect of gravity forces. Proc 27th US Symp Rock Mech (USRMS), Tuscaloosa, Alabama, 789–794

Brouard B, Zakharov V, Frangi A (2022) Numerical modeling of the complex behavior of salt caverns. Int Geomech Symp, Abu Dhabi. https://doi.org/10.56952/IGS-2022-028

Coates GK, Lee CA, McLain WC, Senseny PE (1983) - Closure and Collapse of Man-Made Cavities in Salt. Proc. 6th Int. Symp. Salt, 139-157

Crotogino F, Mohmeyer KU, Scharf R (2001) - Huntorf CAES: More than 20 Years of Successful Operation. SMRI Spring Meeting, Orlando, Florida, 351-362

DeVries KL, Mellegard KD, Callahan GD (2003) Laboratory testing in support of a bedded salt failure criterion. SMRI Fall Tech Conf, Chester, United Kingdom, 90–113

Djizanne H, Bérest P, Brouard B (2014) The mechanical stability of a salt cavern used for compressed air energy storage (CAES). SMRI Spring Tech Conf, San Antonio, TX, USA

Djizanne H, Brouard B, Hévin G (2023) Mechanical stability of a salt cavern used for hydrogen storage. In: 15th ISRM Congress 2023 & 72nd Geomechanics Colloquium. Schubert & Kluckner, 2752–2757

Fracsima (2016) Disroc, a finite element code for modeling thermo-hydro-mechanical processes in fractures porous media

Norton HF (1929) Creep of steel at high temperature. McGraw-Hill, New York, 67 p.

Ouraga Z, Guy N, Pouya A (2017). Modeling of natural fracture initiation and propagation in basin sedimentation context, J. Geophys. Res. Solid Earth, 122, 247–261, doi :10.1002/2016JB013511

Pouya A, Bemani YP (2015) A damage-plasticity model for cohesive fractures. Int J Rock Mech Min Sci 73 :194–202

Röhr H.U (1974) - Mechanical behavior of a gas storage cavern in evaporitic rocks. Proc. 4th Symp. on Salt, A.H. Coogan ed., Salt Institute, II, 93-100

Quast P (1983) L'installation de Huntorf : plus de trois années de fonctionnement de cavernes à air comprimé. Ann Mines 190(5–6):93–102

Tounsi H, Pouya A, Rohmer J (2020) Coupled hydro-chemo-mechanical model for fault activation under reactive fluid injection. Eur J Environ Civil Eng. https://doi.org/10.1080/19648189.2020.1832583